Gervasi *et al. Cell Communication and Signaling* (2025) 23:512
https://doi.org/10.1186/s12964-025-02523-2

Cell Communication and Signaling

RESEARCH Open Access

Mitochondrial connexin 43 modulates metabolic stress adaptation in glioma cell lines

Anna Gervasi[1], Simona Denaro[1], Simona D'Aprile[1,2], Maja Potokar[3,4], Jernej Jorgačevski[3,4], Robert Zorec[3,4], Daniele Tibullo[5], Agata Zappalà[1], Angela Maria Amorini[5], Rosalba Parenti[1*] and Nunzio Vicario[1*]

Abstract

Background Connexin 43 (CX43) is a hemichannel (HC)- and gap junction (GJ)-forming protein that mediates the exchange of small molecules between the intracellular and extracellular environments, as well as intercellular communication. In addition to this canonical role, recent studies have shown that its functions range from transcriptional regulation to intracellular homeostasis. The ability of CX43 to translocate into mitochondria suggests its involvement in energy metabolism. However, the functions of mitochondrial CX43 (mt-CX43) in neural cells remain unexplored.

Methods Our study investigated the expression and localisation of mt-CX43 through western blot and immunofluorescence analyses in four immortalised human glioma cell lines: T98-G, A-172, CCF-STTG1, and U-87 MG. Additionally, targeted metabolomic analysis was conducted to assess changes in key metabolic pathways.

Results Basal CX43 expression and extracellular stress factors, particularly cell density and extracellular pH fluctuations, significantly modulated the mitochondrial localisation of CX43. Inhibition of the heat shock protein 90 (HSP90) chaperone system by geldanamycin (GA) resulted in a marked reduction in mt-CX43, suggesting an import mechanism involving HSP90 and the translocase of the outer membrane (TOM) complex. In addition, the assessment of key metabolites revealed increased purine biosynthesis in T98-G cells exposed to GA treatment, characterised by lower basal CX43 expression and reduced mt-CX43 levels under stress conditions. Conversely, U-87 MG cells exhibited a stable NAD^+/NADH ratio and a significant increase in NADH levels, indicating a metabolic shift towards a more resilient state.

Conclusions Our results suggest that mt-CX43 serves as a multifunctional regulator of metabolic adaptation and stress response in glioma cell lines. Our results extend the role of mt-CX43 as an essential factor in cellular metabolic plasticity, providing new insights into the modulation of metabolic imbalances and mitochondrial dysfunction.

*Correspondence:
Rosalba Parenti
parenti@unict.it
Nunzio Vicario
nunzio.vicario@unict.it

Full list of author information is available at the end of the article

© The Author(s) 2025. **Open Access** This article is licensed under a Creative Commons Attribution-NonCommercial-NoDerivatives 4.0 International License, which permits any non-commercial use, sharing, distribution and reproduction in any medium or format, as long as you give appropriate credit to the original author(s) and the source, provide a link to the Creative Commons licence, and indicate if you modified the licensed material. You do not have permission under this licence to share adapted material derived from this article or parts of it. The images or other third party material in this article are included in the article's Creative Commons licence, unless indicated otherwise in a credit line to the material. If material is not included in the article's Creative Commons licence and your intended use is not permitted by statutory regulation or exceeds the permitted use, you will need to obtain permission directly from the copyright holder. To view a copy of this licence, visit http://creativecommons.org/licenses/by-nc-nd/4.0/.

Plain english summary
Connexin 43 (CX43) is a multifunctional protein known for its canonical role in forming hemichannels and gap junctions, which mediate the exchange of signals and small molecules. Although this pore-forming function occurs primarily at the plasma membrane, CX43 is also localised within mitochondria, suggesting a role in cellular adaptation to energy demands and environmental stress. In this study, we investigated the role of mitochondrial CX43 (mt-CX43) in glioma cell lines. We found that mt-CX43 levels vary depending on cell density and extracellular pH. Furthermore, the import of CX43 into mitochondria requires a transport system involving heat shock protein 90 (HSP90). Inhibition of this system with geldanamycin caused a consistent reduction in mt-CX43, which was associated with alterations in mitochondrial structure and metabolic pathways, including purine metabolism and NADH turnover. Our findings suggest that mt-CX43 is required for cellular adaptation to metabolic stress and that modulating mt-CX43 may represent a novel strategy to disrupt tumour survival mechanisms and improve glioma treatment.

Keywords CX43, Glioblastoma, Geldanamycin, pH, Metabolism, Purine

Introduction

Connexins (CXs) are a family of proteins that regulate intercellular communication by mediating the exchange of ions, second messengers and small molecules between cells and the extracellular environment [1–3]. In the central nervous system (CNS), various CX isoforms are expressed, with connexin 43 (CX43) playing a central role in hemichannels (HCs) and gap junctions (GJs) coupling. CX43, encoded by the *GJA1* gene, is one of the most abundantly expressed connexin isoforms in the CNS, enabling direct cell-to-cell signalling and maintaining intracellular and extracellular homeostasis [4–6]. Recent studies have shown that beyond its canonical role, CX43 is also present within mitochondria (i.e., mt-CX43), suggesting a novel function in mediating mitochondrial dynamics and cellular metabolism [7]. Previous studies have mainly focused on the role of mt-CX43 in cardiomyocytes, where it is thought to be involved in HC formation and regulation of mitochondrial potassium uptake, reactive oxygen species (ROS) generation and energy metabolism [8–10]. Despite this evidence, the role of mt-CX43 in the CNS remains largely unexplored. Given the distinct metabolic requirements and signalling of neural cells, particularly in glial cells, there is growing interest in understanding how mt-CX43 contributes to mitochondrial function in this context [11]. This phenomenon is especially relevant in high-grade gliomas, such as glioblastoma (GBM), an aggressive and resistant tumour characterised by pronounced metabolic plasticity and adaptation to environmental constraints such as hypoxia, acidification, and nutrient deprivation [12–15]. CX43 is variably expressed in gliomas, and its levels have been correlated with both tumour survival and proliferation [16]. This highlights the importance of determining the subcellular localisation and function of CX43, rather than merely its total expression levels [17].

To evaluate the involvement of mt-CX43 in mitochondrial homeostasis and metabolism, it is crucial to assess potential changes in mt-CX43 resulting from alterations in the extracellular environment. Notably, the formation of GJs and the turnover of CX43 proteins are modulated by environmental conditions in gliomas, with cell-to-cell communication being critical for proliferation and self-renewal [18, 19]. For instance, densely packed regions of GBM are characterised by increased cell-to-cell contacts, which are typical of a hyperproliferative tumour microenvironment. This can activate kinases such as protein kinase A (PKA) that phosphorylate specific serine residues on CX43, thereby promoting its assembly into GJ plaques and enhancing intercellular communication [20]. Conversely, in tumour regions characterised by low density, reduced intercellular contact can alter intracellular signalling and promote CX43 phosphorylation at specific sites; these modifications have been directly linked to GJ disassembly and protein internalisation [21]. CX43-based GJs are also sensitive to pH and undergo conformational changes in response to extracellular acidification, leading to channel closure and loss of intercellular communication [22–24]. This is typical of the glioma microenvironment, where the extracellular pH remains acidic because of hypoxia and increased glycolysis [14, 25]. Here, chronic acidosis likely contributes to persistent GJs occlusion and disrupts coordinated intercellular signalling among tumour cells.

Studies have shown that acidic pH not only impairs the function of GJs but also modulates the localisation and expression of CX43 [26]. Therefore, the acidic tumour microenvironment reduces classical GJ-mediated communication and redirects CX43 to non-canonical functions associated with glioma plasticity, invasiveness, and resistance to metabolic stress. Although these data provide valuable insights, the role of extracellular pH fluctuations associated with mt-CX43 in the CNS is still unknown and requires further investigation. These pivotal observations prompted us to hypothesise that a proportion of internalised CX43, induced by cell density or stressors, may be redirected to intracellular

compartments, including mitochondria, and that this process is dynamically regulated by cells in response to their physiological state.

To investigate the contribution of mt-CX43 to metabolic adaptation, we selected four human glioma cell lines (i.e., T98-G, A-172, CCF-STTG1, and U-87 MG), based on their differential *GJA1* expression levels. This choice allowed us to compare cell lines with low, intermediate and high levels of CX43 and to test whether basal CX43 abundance correlates with its mitochondrial localisation and functional role under stress conditions.

We also modulated the internalisation of CX43 into mitochondria by inducing extracellular pH shifts (i.e., alkaline and acidic), with different results depending on the cell line. Moreover, we combined pH modulation with treatment with geldanamycin (GA), a heat shock protein 90 (HSP90) inhibitor known to impair the import of CX43 into mitochondria by disrupting the HSP90-TOM complex [27, 28]. We observed a shift towards increased purine biosynthesis in T98-G cells and purine degradation in U-87 MG cells upon GA treatment. Our data suggest that the function of mt-CX43 is critical for CNS cell homeostasis and for modulating the cellular response to extracellular stressors, opening potential avenues for treating mitochondrial dysfunction in CNS diseases.

Methods

Selection and analysis of CNS cell line dataset

RNA-seq gene expression data from CNS cancer cell lines were obtained from the Cancer Cell Line Encyclopedia (CCLE) and analysed using the UCSC's Xena browser (https://xenabrowser.net/, accessed in April 2025). Genes of interest encoding 19 connexins (i.e., *GJA1*, *GJA3*, *GJC1*, *GJC2*, *GJC3*, *GJB5*, *GJB2*, *GJB3*, *GJB4*, *GJA5*, *GJB6*, *GJB7*, *GJB1*, *GJA4*, *GJD4*, *GJD2*, *GJA10*, *GJA8*, *GJE1*) were selected for further analysis. Gene expression values were retrieved in reads per kilobase of transcript per million mapped reads (RPKM).

Cell culture and drug administration

The experiments were performed using the following human cell lines: T98-G (Cat. No. #CRL-1690, RRID: CVCL_0556, ATCC), A-172 (Cat. No. #CRL-1620, RRID: CVCL_0131, ATCC), CCF-STTG1 (Cat. No. #CRL-1718, RRID: CVCL_1118, ATCC), and U-87 MG (Cat. No. #HTB-14, RRID: CVCL_0022, ATCC).

The cell lines were cultured at 37 °C in a humidified atmosphere, 5% CO_2, and were routinely sub-cultured into standard culture flasks. Mycoplasma negative cells with a passage < 25 were used in this study. For T98-G and U-87 MG cells, the complete growth medium consisted of: 10% foetal bovine serum (FBS, Cat. No. #26140079, Gibco), 100 IU/ml penicillin-streptomycin (pen-strep, Cat. No. #15140-122, Gibco), 1 mmol/l sodium pyruvate (Cat. No. #11360-039, Gibco), 1 mmol/l non-essential amino acids (Cat. No. #11140-050, Gibco), and 1 mmol/l L-glutamine (Cat. No. #25030-081, Gibco) in minimum essential medium (MEM) (Cat. No. #ECB2071L, Euroclone). For A-172 cells, the complete growth medium consisted of: 10% FBS (Cat. No. #26140079, Gibco), 1% pen-strep 100 IU/ml (Cat. No. #15140-122, Gibco), 1 mmol/l sodium pyruvate (Cat. No. #11360-039, Gibco), and 1 mmol/l L-glutamine (Cat. No. #25030-081, Gibco) in Dulbecco's modified Eagle medium (DMEM) supplemented with 4.5 g/L D-glucose (Cat. No. #11965092, Gibco). For CCF-STTG1 cells, the complete growth medium consisted of: 10% FBS (Cat. No. #26140079, Gibco), 100 IU/ml pen-strep (Cat. No. #15140-122, Gibco), 1 mmol/l sodium pyruvate (Cat. No. #11360-039, Gibco), in RPMI supplemented with 2.5 g/L D-glucose (Cat. No. #ECB2000L, Euroclone).

To assess the effects of plating density, low plating density (LD) experiments were performed with cells plated at a final density of 20,000 cells per cm^2, medium plating density (MD) experiments were performed by plating cells at a final density of 40,000 cells per cm^2, and high plating density (HD) experiments were performed by plating cells at a final density of 80,000 cells per cm^2.

Extracellular pH alterations were induced by adding an appropriate amount of hydrochloric acid (HCl) (Cat. No. #403871, Carlo Erba reagents) or sodium hydroxide (NaOH) (Cat. No. #S5881, Sigma-Aldrich) to bring the pH steadily to pH = 6.0 or pH = 8.0. The culture media were first supplemented with HCl or NaOH and then incubated for 24 h at 37 °C in a humidified atmosphere and 5% CO_2. The pH was verified at this stage to ensure that CO_2 levels did not alter the pH. All pH = 6.0 media had a mean pH ± SD of 6.0 ± 0.1, and pH = 8.0 media had a mean pH ± SD of 8.0 ± 0.1.

For lactate treatment, cells were treated with sodium L-lactate (Cat. No. #71718-10G, Sigma-Aldrich) at a final concentration of 20 µM in the growth medium for 24 h. For GA treatment, cells were treated with GA (Cat. No. #J63397.MB, ThermoScientific Chemicals) at a final concentration of 10 µM in dimethyl sulfoxide (DMSO) for 30 min. Control cultures were treated with an equivalent amount of vehicle (i.e., growth medium or DMSO). In DMSO-exposed cultures (with/without GA) the total amount of DMSO was < 1%.

Western blot analysis and isolation of mitochondria

For Western blot analysis, cells were plated at either LD (20,000 cells per cm^2), MD (40,000 cells per cm^2) or HD (80,000 cells per cm^2). After 12 h, the cells were treated with either the vehicle or 20 µM sodium L-lactate for an additional 24 h. The cell medium was then removed, and the cultures were washed with PBS. The cells were detached using a cell scraper (Cat. No. #CLS353087,

Merck). Pellets were obtained by centrifugation at 300 × g for 5 min, and either the total protein content or the mitochondrial protein content was isolated. Total protein content was obtained by incubating the cell pellets with RIPA buffer (Cat. No. #R0278, Sigma-Aldrich) supplemented with protease inhibitor (1:100, Cat. No. #P8340, Merck) at 4 °C for 20 min. The suspension was then centrifuged at 13,000 × g for 5 min at 4 °C, and supernatants were collected in a new series of tubes. Mitochondrial protein content was obtained using the Mitochondria Isolation Kit (Cat. No. ab11017, Abcam), according to the manufacturer's instructions. Briefly, cells were collected using a cell scraper and centrifuged at 1,000 × g for 10 min. The cell pellets were frozen and thawed to weaken the cell membranes, resuspended in reagent A and incubated at 4 °C for 10 min. Homogenisation was performed according to the manufacturer's instructions. The homogenates were centrifuged at 1,000 × g for 10 min at 4 °C, and the supernatant was collected in a new set of tubes. This procedure was repeated with the pellets using reagent B. The combined supernatants from both steps were pooled together and centrifuged at 12,000 × g for 15 min at 4 °C to obtain isolated mitochondria. The total mitochondrial protein content was recovered by resuspending the mitochondria in reagent C supplemented with protease inhibitors and stored at – 80 °C until use.

Equal amounts of protein were electrophoresed and transferred to nitrocellulose membranes (Cat. No. #1704158, Bio-Rad). The membranes were blocked with 5% non-fat milk (Cat. No. #A0830,0500, ITW Reagents) in 0.1% Tween-20 (Cat. No. #P9416, Sigma-Aldrich) in PBS for 1 h and incubated overnight at 4 °C with the following primary antibodies: 1:1,000 rabbit anti-Connexin 43 (Cat. No. #C6219, RRID: AB_476857, Sigma-Aldrich), 1:1,000 mouse anti-β-actin (Cat. No. #sc-47778, RRID: AB_2714189, Santa Cruz Biotechnology), 1:10,000 mouse anti-SDHA (Cat. No. #ab14715, RRID: AB_301433, Abcam). The following day, the membranes were washed with 0.1% Tween-20 in PBS and then incubated with appropriate HRP-conjugated secondary antibodies: 1:5,000 goat anti-mouse IgG (H + L) (Cat. No. #31430, RRID: AB_228307, Invitrogen); 1:10,000 goat anti-rabbit IgG (H + L) (Cat. No. #31460, RRID: AB_228341, Invitrogen). Bands were detected using a ChemiDoc Imaging System (Bio-Rad) and densitometric analysis was performed using ImageJ software. The relative expression levels of CX43 or mt-CX43 were determined by dividing the intensity of CX43 or mt-CX43 bands by the intensity of β-ACTIN or SDHA of the same membrane. Uncropped membranes are shown in the supplementary information file – Uncropped Gels and Blots images.

For the time-course experiment on pH-dependent mt-CX43 expression and to evaluate the temporal dynamics of CX43 mitochondrial translocation after alkalinisation, cells were exposed to extracellular medium adjusted to pH = 6.0 for 12 h, and then pH was shifted to pH = 8.0 by complete medium change. Mitochondrial fractions were isolated as described above at 0, 30, 60, 120 and 180 min and subjected to western blotting for mt-CX43 quantifications. Relative mt-CX43 levels were calculated as fold change over time 0.

Immunofluorescence staining

For immunofluorescence analysis, cells were seeded on 24-well plates with 12 mm coverslips at a final density of 20,000 cells per cm^2 (i.e., LD) or 80,000 cells per cm^2 (i.e., HD) and incubated for 12 h at 37 °C and 5% CO_2. Cells were treated with either vehicle or GA and exposed to extracellular pH alterations (i.e., pH = 6.0, pH = 7.0, or pH = 8.0). At specific time points, the medium was removed, cells were rinsed with PBS, and fixed with 4% paraformaldehyde (PFA, Cat. No. #158127, Sigma-Aldrich) for 10 min at room temperature. The PFA was then removed, the cells were washed in PBS and stored at 4 °C until use.

Immunocytochemistry was performed as previously described [29, 30]. Briefly, fixed cells were rinsed in PBS and then blocked with 10% normal goat serum (NGS, Cat. No. #16210064, ThermoFisher Scientific), and 0.1% Triton X-100 (Cat. No. #93443, Sigma-Aldrich) in PBS for 1 h at room temperature. Samples were then incubated with the following primary antibodies: rabbit anti-Connexin 43 (1:100, Cat. No. #C6219, RRID: AB_476857, Sigma-Aldrich), mouse anti-mitochondria (1:100, Cat. No. #ab92824, RRID: AB_10562769, Abcam) overnight at 4 °C. The following day, samples were washed three times with 0.1% Triton X-100 in PBS and incubated for 1 h at room temperature with the appropriate combination of the following fluorescent secondary antibodies diluted in 0.1% Triton X-100 in PBS: goat anti-mouse Alexa Fluor-546 (1:1,000, Cat. No. #A11003, RRID: AB_141370, Invitrogen), goat anti-rabbit Alexa Fluor-647 (1:1,000, Cat. No. #A21244, RRID: AB_2535812, Invitrogen).

After incubation, samples were washed three times with 0.1% Triton X-100 in PBS, and F-actin was stained with Alexa Fluor 488 Phalloidin (PHD, 1:300, Cat. No. #A12379, Invitrogen). Samples were washed, and nuclei were counterstained with DAPI (Cat. No. #D1306, Invitrogen). Coverslips were mounted with Fluoromount TM Aqueous Mounting Medium (Cat. No. #F4680, Sigma-Aldrich), and images were acquired using a Leica TCS SP8 confocal microscope.

Quantification of CX43 distribution, colocalisation and mitochondrial morphological parameters

To analyse the intracellular distribution of CX43, confocal microscopy images were processed using Fiji software (v. 2.16.0/1.54p) [31]. Images were acquired from at least

five randomly selected regions of interest (ROIs) per coverslip. Z-stack images were acquired, the cell perimeter was outlined using the selection tool, and the total cell area was quantified. For subcellular distribution, subplasmalemmal and nuclear regions were segmented based on their proportional relationship to the total cell area. The subplasmalemmal region was estimated as 30% of the total cell area, while the nuclear region was defined using the selection tool and a nuclear region with DAPI-positive area was drawn as a reference.

On a selected region of interest (ROI, i.e., subplasmalemmal and nuclear), the CX43 distribution was evaluated using the LPX Filter2d plugin using the "Fftswap" filter. Quantification of pixel intensity was performed for each compartment, and data were normalised to the total CX43 intensity.

Colocalisation analysis of CX43 with the mitochondrial marker was assessed using the Coloc 2 plugin in Fiji software (v. 2.16.0/1.54p). Pearson's correlation coefficient was calculated on dual-channel confocal immunofluorescence images to determine the spatial colocalisation between CX43 and mitochondria. To ensure the robustness of colocalisation analysis, a total number of $n \geq 18$ cells from $n \geq 3$ biological replicates were quantified.

Morphological analysis of stained mitochondria was performed with the Mitochondria Analyser plugin [32], run in Fiji, version 2.14.0/1.54p [31]. To describe the morphology of the mitochondria, the total number of individual mitochondrial particles and the total branch length/mito were calculated.

Targeted metabolomics and metabolite ratio analysis

For the analysis of metabolites, cells were trypsinized, resuspended in PBS (1×10^6 cells/ml) and centrifuged at 300 × g for 5 min at room temperature. The resulting cell pellet was deproteinized using a precipitation solution containing 75% acetonitrile and 25% KH_2PO_4, (10 mM, pH = 7.4) followed by centrifugation at 20,890 g for 10 min at 4 °C. The obtained supernatant was mixed with chloroform to extract the aqueous phase. The selected metabolites were separated using a C18 chromatography column (Hypersil C-18, 250 × 4.6 mm, 5 µm particle size) integrated with a high-performance liquid chromatography (HPLC) system (ThermoFisher Scientific, Vanquish LC System). A diode-array detector HL (Thermo Fisher Scientific) at wavelengths of 206 nm and 260 nm was used for the identification and quantification of metabolites.

Principal component analysis

Principal component analysis (PCA) was conducted using the metabolite data. A scree plot was generated, displaying the variance explained by each component, and a correlation plot showing the contributions of the principal components (PCs) as cosine squared (cos^2). The PCA results are shown as a biplot, with each variable represented by coloured arrows. All analyses were performed using RStudio software (Version: 2024.09.1 + 394).

Statistical analysis

Data analysis was performed using GraphPad Prism software version 8.0.1. The sample size for each experiment is reported in the figure legends. Quantifications were performed by operators blinded to the treatment, and no data points were excluded from the analysis *ex-ante*. Outliers were identified using the ROUT method with a Q = 1%. Data were assessed for normal distribution by using the Shapiro–Wilk test or the D'Agostino & Pearson test, depending on sample size, followed by evaluation of homogeneity of variance. Datasets that passed both tests were analysed with a two-tailed unpaired Student's t-test for comparisons of $n = 2$ groups, or one-way or two-way analysis of variance (ANOVA), followed by the Holm-Sidak post hoc test for multiple comparisons, for comparison of $n \geq 3$ groups.

Datasets with non-normal distribution were analysed using the Kruskal–Wallis test. Data are presented as the mean or mean fold change (FC) ± standard deviation (SD). For all statistical tests, p-values < 0.05 were considered statistically significant.

Results

Mitochondrial localisation of CX43 is regulated by cell density and the baseline expression of CX43

To determine differences among glioma cell lines with respect to baseline CXs expression, we first performed a transcriptomic analysis using a publicly available dataset via UCSC Xena (Fig. 1a).

Our analyses showed that the mRNA levels of CXs isoforms were heterogeneously expressed in the CNS cell lines, with *GJA1*, encoding CX43, having an average raw reads per kilobase per million (RPKM) of approximately 49.22 among all available cell lines. Interestingly, *GJC1*, encoding CX45, was the second most highly expressed gene with an average RPKM of 7.44. All other CX genes analysed were markedly less expressed in the CNS cell lines, with an average RPKM of approximately 0.09, or were undetectable. Based on *GJA1* expression, we selected four glioma cell lines exhibiting low, medium, or high *GJA1* expression levels, namely T98-G (33.40 RPKM; low), A-172 and CCF-STTG1 (46.31 RPKM for A-172; 79.54 RPKM for CCF-STTG1; intermediate), and U-87 MG (132.80 RPKM for U-87 MG; high; Fig. 1a).

To test protein levels and the potential effects of plating cell density (i.e., low density, LD; medium density, MD; and high density, HD), total CX43 expression levels

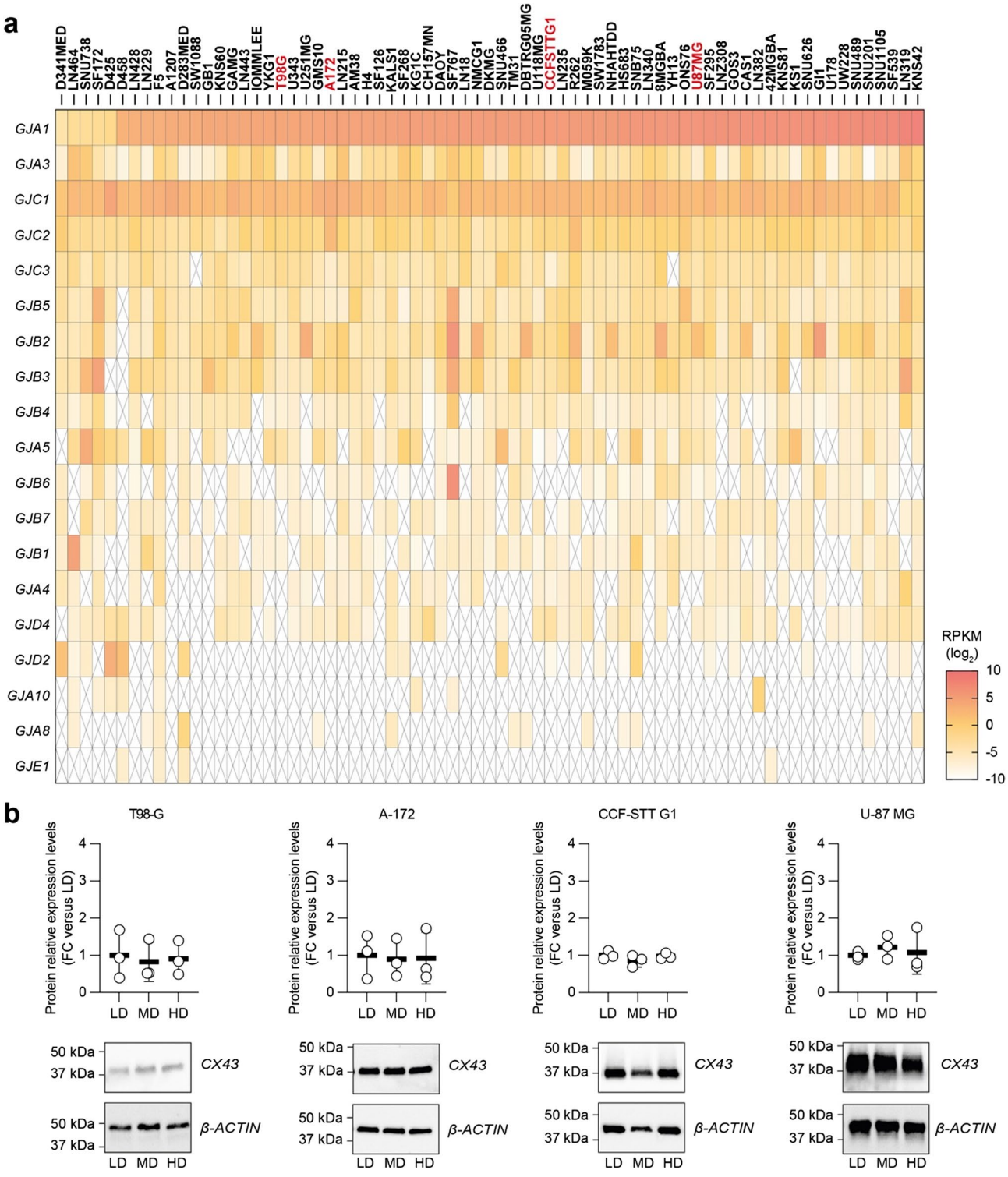

Fig. 1 Connexin isoforms are heterogeneously expressed in glioma cell lines. **a** Heatmap showing RNA-seq data from publicly available datasets on the expression levels of CX isoforms in glioma cell lines, expressed as $\log_2$ RPKM. The cells are ordered by abundance in *GJA1*. Unavailable/not-detected data are marked with a cross. Cell lines marked in red were selected for further experiments. **b** Western blot analysis of total protein expression of CX43 in T98-G, A-172, CCF-STTG1 and U-87 MG cell lines cultured under LD, MD, and HD. Data are presented as dot plot and mean ± SD of FC versus LD from $n = 3$ independent replicates. RPKM: reads per kilobase per million; LD: low density; MD: medium density; HD: high density; FC: fold change

were assessed by Western blot analysis (Fig. 1b). Our data showed that there were no significant changes in total CX43 levels among LD, MD, and HD in all cell lines tested at 24 h (Fig. 1b).

To assess the effect of potential stressors or inducers on CX43 expression levels, T98-G, A-172, CCF-STTG1, and U-87 MG cells were exposed to extracellular L-lactate in either LD or HD. We first assessed the total protein content of LD and HD cultures in control and lactate-treated cells. Our results showed no significant changes in any of the conditions or cell lines tested (Fig. 2a-d), suggesting that total CX43 expression is not affected by lactate or cell density. We then investigated possible effects of cell density or L-lactate stimulation on mt-CX43.

We found that T98-G and A-172 cells, which are characterised by a relatively lower total CX43 content compared to the other cell lines tested, showed a significant reduction of approximately 40% in mt-CX43 under HD culture conditions (0.60 ± 0.06 in T98-G HD, and 0.60 ± 0.04 in A-172 HD, FC versus LD; Fig. 2e-f). Mt-CX43 expression levels were not significantly affected in CCF-STTG1 cells (Fig. 2g), whereas U-87 MG cells, which are characterised by a higher total CX43 content, showed a 2.40-fold increase in mt-CX43 expression levels when cultured in HD (Fig. 2h).

To further explore intracellular CX43 localisation, we performed confocal-assisted imaging and quantified colocalisation between CX43 and mitochondria in T98-G (Fig. 3a-b), A-172 (Fig. 3c-d), CCF-STTG1 (Fig. 3e-f), and U-87 MG (Fig. 3g-h) cells.

We also assessed the percentage of CX43 occupancy in the subplasmalemmal (Figure S1) and nuclear regions (Figure S2). The results showed a reduction in the proportion of mt-CX43 in CX43 low-expressing cell lines (i.e., T98-G and A-172) under HD culture conditions, compared to LD (0.24 ± 0.07 HD T98-G vs. 0.51 ± 0.08 LD T98-G; 0.33 ± 0.11 HD A-172 vs. 0.46 ± 0.08 LD A-172; Fig. 3a-d), and a significant increase in mt-CX43 in the HD U-87 MG cell line (0.49 ± 0.09 HD U-87 MG vs. 0.29 ± 0.11 LD U-87 MG; Fig. 3g-h). In CCF-STTG1 cells, no significant changes in mt-CX43 were observed between LD and HD (0.31 ± 0.10 HD CCF-STTG1 vs. 0.30 ± 0.13 LD CCF-STTG1; Fig. 3e-f). Interestingly, the subplasmalemmal fraction of CX43 was significantly affected by cell density in A-172 cells (3.51 ± 2.46 HD A-172 vs. 0.62 ± 0.32 LD A-172; Figure S1), and in CCF-STTG1 cells (2.29 ± 1.37 HD CCF-STTG1 vs. 0.26 ± 0.13 LD CCF-STTG1; Figure S1). In contrast, the nuclear fraction was significantly increased in HD CCF-STTG1 cells (5.74 ± 3.18 HD CCF-STTG1 vs. 1.47 ± 1.14 LD CCF-STTG1; Figure S2), with no significant changes in any of the other cell lines tested.

High-density cultures promote mitochondrial fusion in T98-G cells and fission in U-87 MG cells

Given the changes in mitochondrial CX43 localisation, we investigated whether mitochondrial morphology was similarly affected (Figure S3). Our analysis revealed that T98-G cells remodelled the mitochondrial network under HD conditions by significantly reducing the number of individual mitochondrial particles (0.54 ± 0.28 HD T98-G, FC versus LD; Fig. 4a-b) and increasing the total length of branches per mitochondrion (2.51 ± 1.60 HD T98-G, FC versus LD; Fig. 4a-b). The A-172 cell line showed minimal changes in mitochondrial morphology and network, with a slight increase in the total number of individual mitochondrial particles (1.63 ± 1.09 HD A-172, FC versus LD; Fig. 4c-d) and no significant changes in mitochondrial branch length per mitochondrion (Fig. 4c-d). CCF-STTG1 cells were characterised by substantial remodelling of mitochondrial content, showing a strong increase in both morphological parameters tested (number of individual mitochondrial particles: 2.03 ± 0.73 HD CCF-STTG1, FC versus LD; total branch length per mitochondrion: 2.21 ± 1.15 HD CCF-STTG1, FC versus LD; Fig. 4e-f). Importantly, HD U-87 MG cells, characterised by increased mt-CX43 content, showed a significant increase in the number of mitochondrial particles (3.04 ± 1.77 HD U-87 MG, FC versus LD; Fig. 4g-h) in conjunction with a decrease in the total branch length per mitochondrion (0.67 ± 0.26 HD U-87 MG, FC versus LD; Fig. 4g-h). These observations were supported by a biplot correlation analysis of the number of mitochondrial particles and the total branch length per mitochondrion, which showed that the observed morphological changes were consistent with mitochondrial fusion in T98-G cells and mitochondrial fission in U-87 MG cells (Fig. 4i).

Geldanamycin inhibits extracellular pH-mediated translocation of CX43 to the mitochondria

Given the demonstrated modulatory effect of pH alteration on CX43 expression and function [33], we next analysed the effects of acidic (i.e., pH = 6.0) and alkaline (pH = 8.0) extracellular pH alterations on mt-CX43 localisation (Fig. 5a-d).

Our data showed a significant reduction in mt-CX43 expression in T98-G cells exposed to pH = 6.0 (0.53 ± 0.06, FC versus pH = 7.0; Fig. 5a), and near-normal levels when cultured at pH = 8.0 (1.12 ± 0.18, FC versus pH = 7.0; Fig. 5a). This phenomenon was also observed in CCF-STTG1 cells, which showed a significant decrease in mt-CX43 at pH = 6.0 (0.48 ± 0.10, FC versus pH = 7.0; Fig. 5c), and a slight but non-significant increase at pH = 8.0 (1.22 ± 0.12, FC versus pH = 7.0; Fig. 5c). Interestingly, A-172 and U-87 MG cells showed no significant changes in the mt-CX43 expression levels, either at pH = 6.0 (1.06 ± 0.14 A-172

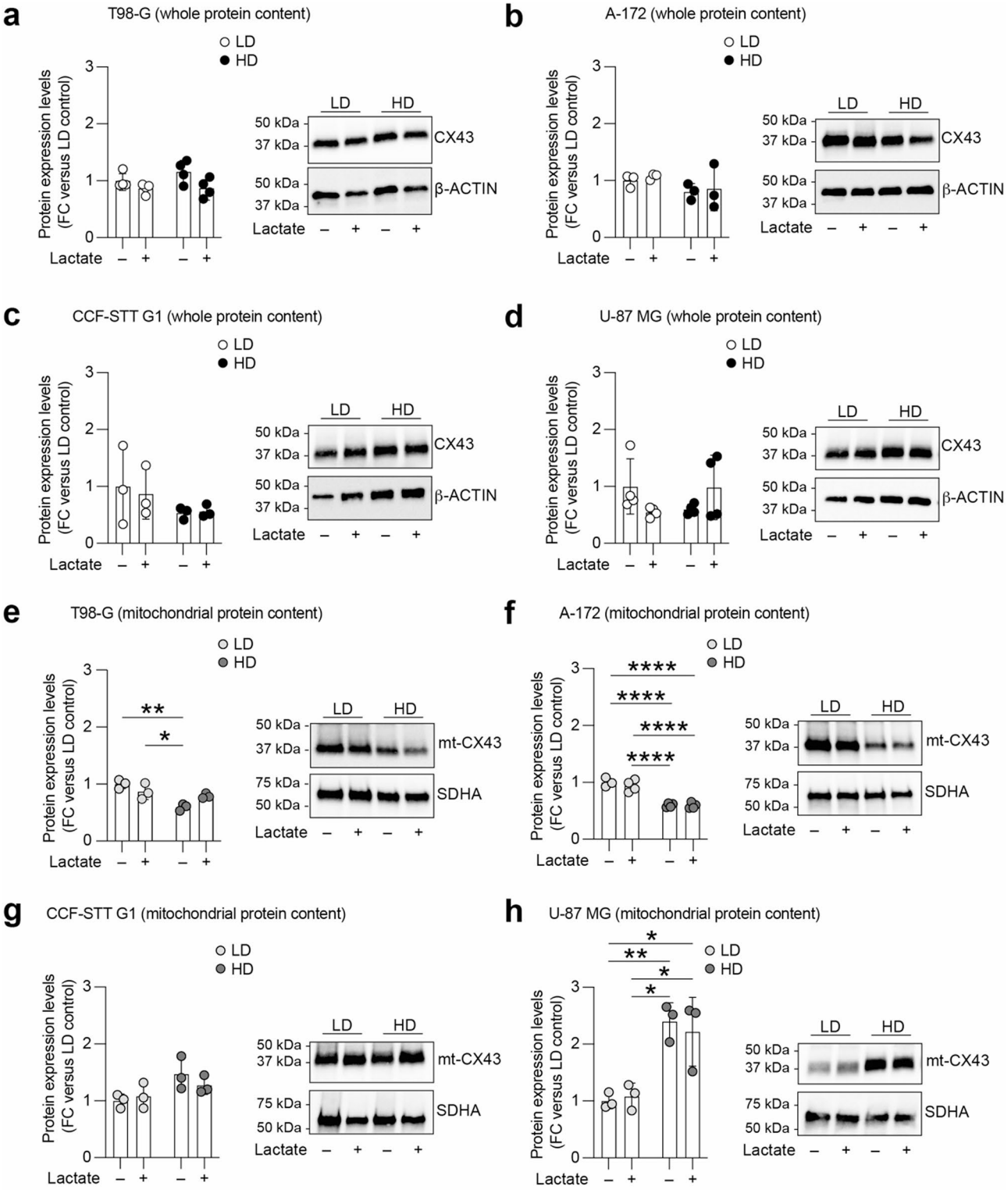

Fig. 2 Mitochondrial localisation of CX43 is affected by cell density and basal expression. **a**-**d** Western blot analysis of total CX43 protein in T98-G (**a**), A-172 (**b**), CCF-STTG1 (**c**), and U-87 MG (**d**) cell lines cultured under LD or HD, and untreated or treated with 20 μM lactate. Data are expressed as mean ± SD of FC versus LD control from $n \geq 3$ independent replicates. **e**-**h** Western blot analysis for CX43 on mitochondrial protein content (mt-CX43) of T98-G (**e**), A-172 (**f**), CCF-STTG1 (**g**), and U-87 MG (**h**) cell lines cultured at LD or HD, untreated or treated with 20 μM lactate. Data are presented as scatter dot plot and mean ± SD of FC versus LD control from $n \geq 3$ independent replicates. *p-value < 0.05; **p-value < 0.01; ****p-value < 0.0001. LD: low density; HD: high density. FC: fold change

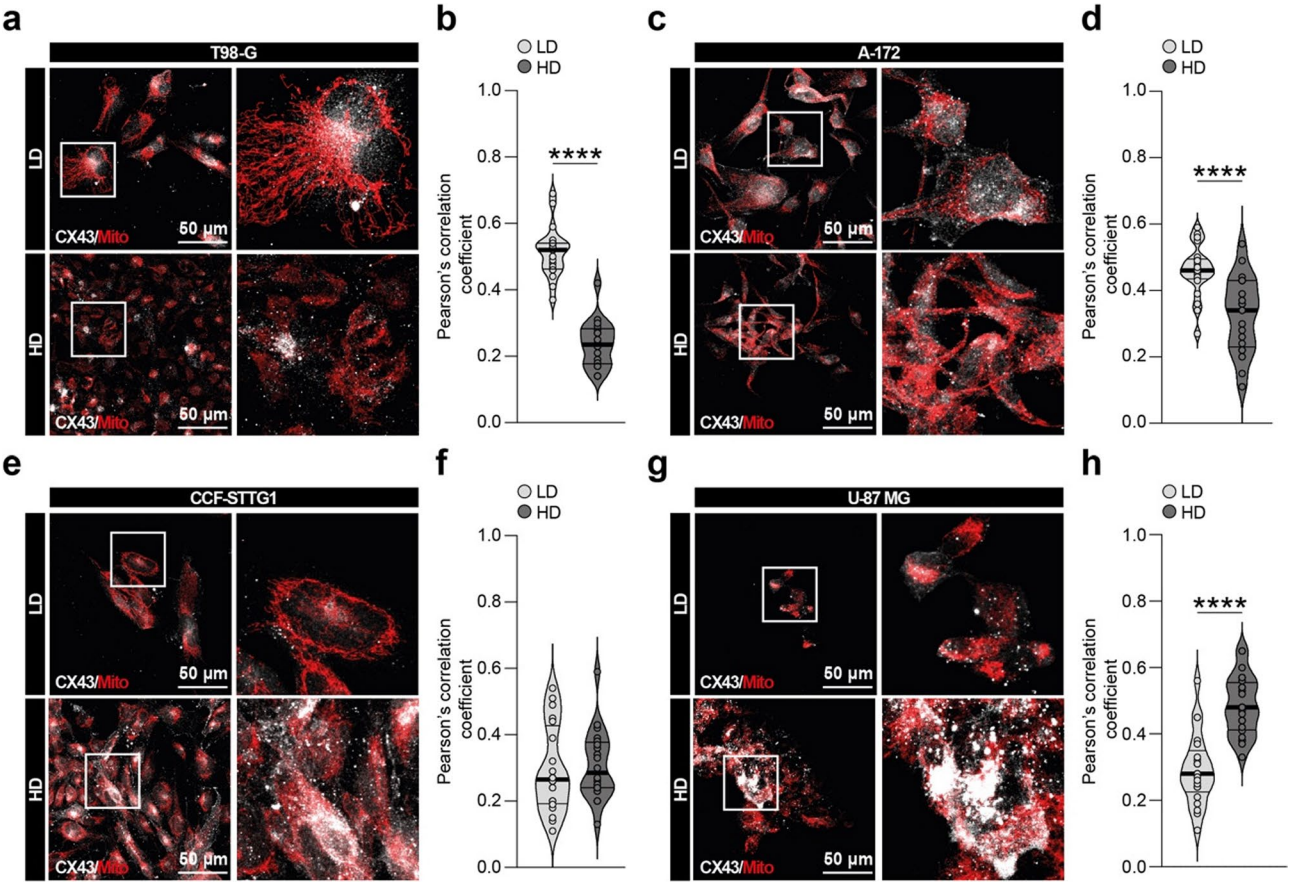

Fig. 3 Mitochondrial localisation of CX43 is reduced in low expressing cell lines at high plating density. **a**-**b** Representative confocal images of CX43 (white) and Mito (red) in LD and HD T98-G cells (**a**) and quantification of Pearson's correlation coefficient (**b**). **c**-**d** Representative confocal images of CX43 (white) and Mito (red) in LD versus HD A-172 cells (**c**) and quantification of Pearson's correlation coefficient (**d**). **e**-**f** Representative confocal images of CX43 (white) and Mito (red) in LD and HD CCF-STTG1 cells (**e**) and quantification of Pearson's correlation coefficient (**f**). **g**-**h** Representative confocal images of CX43 (white) and Mito (red) in LD versus HD U-87 MG cells (**g**) and quantification of Pearson's correlation coefficient (**h**). Data are shown as dot plot and violin plot, with the middle line representing the median and the thin lines the quartiles from $n \geq 3$ biological replicates. ****p-value < 0.0001. Mito: mitochondrial marker; LD: low density; HD: high density.

and 0.87 ± 0.05 U-87 MG, FC versus pH = 7.0; Fig. 5b and d), or at pH = 8.0 (1.12 ± 0.12 A-172 and 1.00 ± 0.15 U-87 MG, FC versus pH = 7.0, Fig. 5b and d).

We extended our analysis to T98-G, assessing the effect of extracellular alkalinisation over time. Here, we found a significant linear correlation between mt-CX43 expression levels and alkalinisation of the extracellular milieu over time ($R^2 = 0.6307$; p-value = 0.0004; Fig. 5e), with an increase in mt-CX43 at 180 min post-alkalinisation of approximately 40% compared with 0 min post-alkalinisation (Fig. 5e).

To modulate CX43 shuttling between the cytoplasm and mitochondria, we exposed cell cultures to an acidic pH for 12 h and then increased the extracellular pH to 8.0, with or without an inhibitor of mitochondrial protein import (i.e., geldanamycin – GA, Fig. 5f). We performed confocal-assisted imaging and quantified the colocalisation of CX43 with mitochondria at pH = 6.0, pH = 8.0, and pH = 8.0 with GA (Fig. 5g-j). We confirmed a significant increase in Pearson's correlation coefficient at pH = 8.0 in T98-G cells (0.43 ± 0.08 pH = 8.0 vs. 0.33 ± 0.09 pH = 6.0, Fig. 5g) and CCF-STTG1 cells (0.27 ± 0.08 pH = 8.0 vs. 0.20 ± 0.08 pH = 6.0, Fig. 5i). At pH = 8.0, no changes were observed in A-172 and U-87 MG compared to the controls at pH = 6.0 (0.44 ± 0.09, pH = 8.0, vs. 0.40 ± 0.05 pH = 6.0 for A-172; 0.35 ± 0.11, pH = 8.0 vs. 0.37 ± 0.15, pH = 6.0 for U-87 MG; Fig. 5h and j). Importantly, GA treatment significantly reduced the proportion of mt-CX43, as evidenced by Pearson's correlation coefficient at pH = 8.0 in all the tested cell lines (0.32 ± 0.09 T-98 G pH = 8.0 + GA, Fig. 5g; 0.33 ± 0.10 A-172 pH = 8.0 + GA, Fig. 5h; 0.21 ± 0.07 CCF-STTG1 pH = 8.0 + GA, Fig. 5i; 0.28 ± 0.11 U-87 MG pH = 8.0 + GA, Fig. 5j). These data confirmed the modulatory effect of GA on suppressing the HSP90-mediated mitochondrial import of CX43.

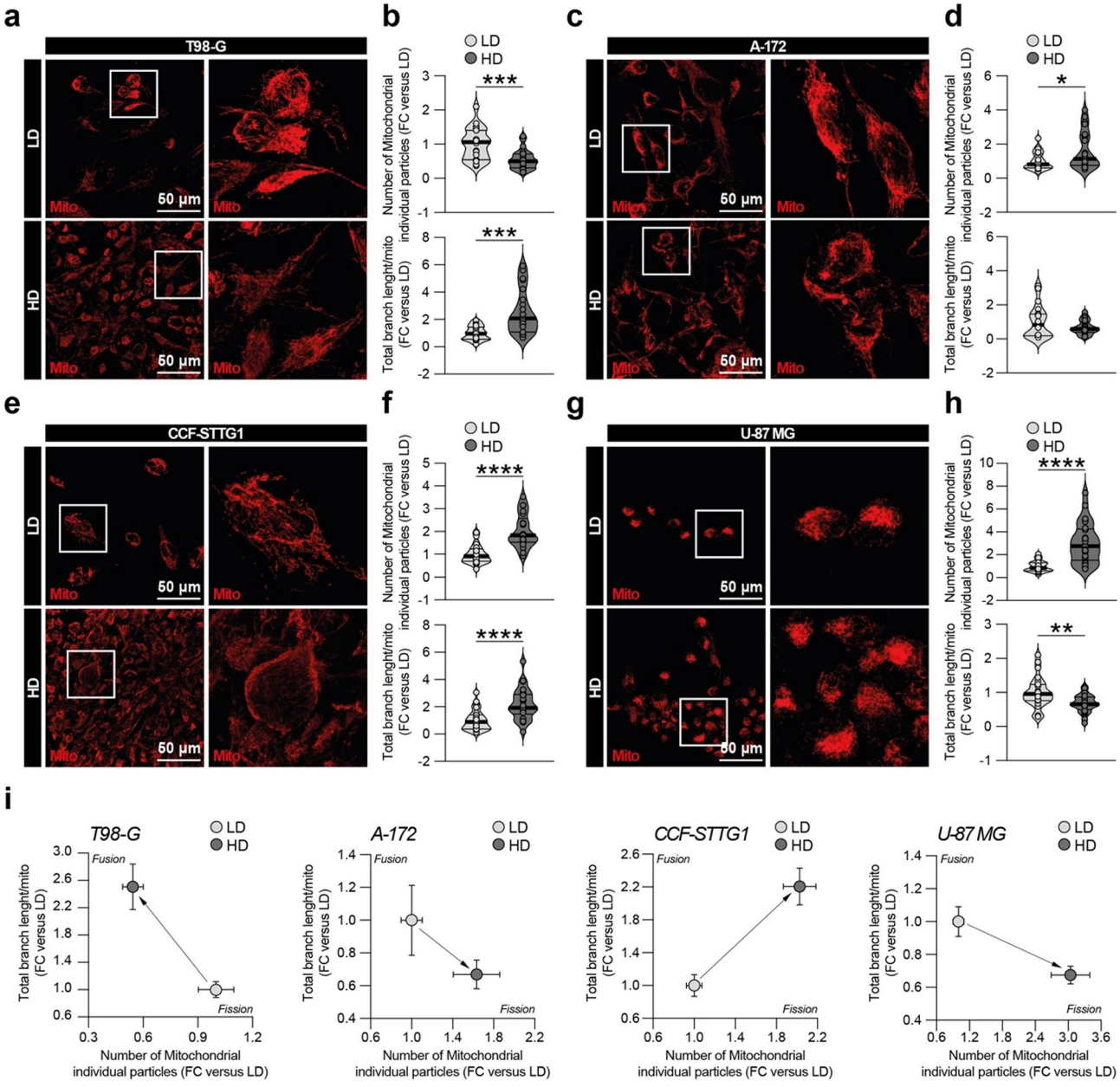

Fig. 4 High-density culture conditions reshape mitochondrial dynamics in T98-G cells and U-87 MG cells. **a**-**b** Representative confocal images of Mito (red) in LD and HD T98-G cells (**a**) and quantification of the number of individual mitochondrial particles and total branch length per mito (**b**). **c**-**d** Representative confocal images of Mito (red) in LD and HD A-172 cells (**c**) and quantification of the number of individual mitochondrial particles and the total branch length per mito (**d**). **e**-**f** Representative confocal images of Mito (red) in LD and HD CCF-STTG1 cells (**e**) and quantification of the number of individual mitochondrial particles and the total branch length per mito (**f**). **g**-**h** Representative confocal images of Mito (red) in LD and HD U-87 MG cells (**g**) and quantification of the number of individual mitochondrial particles and the total branch length per mito (**h**). **i** Biplot analysis of the data in (**b**, **d**, **f** and **h**) for T98-G, A-172, CCF-STTG1, and U-87 MG cells. The arrows indicate the shift of parameters from LD to HD cultures. Data in (**b**, **d**, **f** and **h**) are expressed as FC versus LD and shown as dot plot and violin plot, with the middle line representing the median and the thin lines the quartiles from $n \geq 3$ biological replicates. *p-value < 0.05; **p-value < 0.01; ***p-value < 0.001; ****p-value < 0.0001. Mito: mitochondrial marker; LD: low density; HD: high density; FC: fold change

Mitochondrial CX43 levels are associated with metabolic alterations and recovery from stress

To establish a link between CX43 shuttling and the modulatory effect of GA, we investigated mitochondrial morphology parameters in GA-treated cells compared to control cells cultured at pH = 8.0 (Figure S4). Using immunofluorescence analysis, we quantified individual mitochondrial particles in T98-G after GA treatment and found a significant increase in the total number of individual mitochondrial particles (1.40 ± 0.43 T98-G + GA,

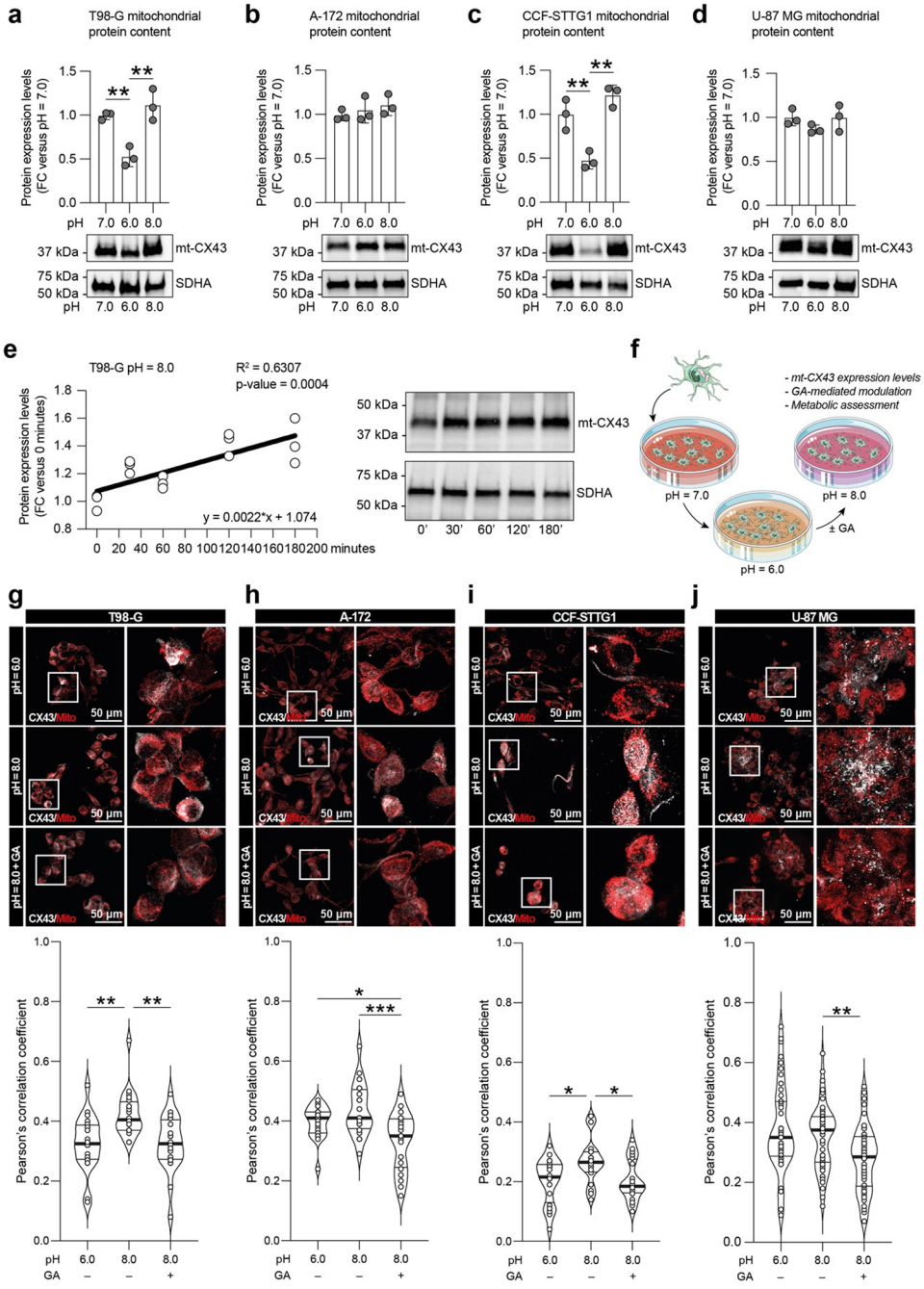

Fig. 5 Geldanamycin inhibits the mitochondrial shuttling of CX43 in cells exposed to alkaline extracellular pH. **a**-**d** Western blot analysis for CX43 on mitochondrial protein levels (mt-CX43) of T98-G (**a**), A-172 (**b**), CCF-STTG1 (**c**), and U-87 MG (**d**) cell lines at pH = 7.0, pH = 6.0, and pH = 8.0. Data are shown as a dot plot and mean ± SD of FC versus pH = 7.0 from $n = 3$ independent replicates. **e** Linear regression analysis of Western blot quantification of mitochondrial protein content (mt-CX43) in T98-G cells exposed to pH = 8.0 at 0, 30, 60, 120, and 180 min. Data are shown as a dot plot of FC versus pH = 6.0 and as a dot plot from $n = 3$ independent replicates. R-squared, p-value, and equation of the linear regression analysis are reported. **f**) Schematic representation of the experimental setup for GA treatment and mt-CX43 assessment. **g**-**j**) Representative confocal images of CX43 (white) and Mito (red) at pH = 6.0, pH = 8.0, and pH = 8.0 + GA and quantification of Pearson's correlation coefficient of T98-G (**g**), A-172 (**h**), CCF-STTG1 (**i**), and U-87 MG (**j**) cell lines. Data are shown as dot plot and violin plot, with the middle line representing the median and the thin lines the quartiles from $n \geq 3$ biological replicates. *p-value < 0.05; **p-value < 0.01; ***p-value < 0.001. Mito: mitochondrial marker; GA: geldanamycin; FC: fold change

FC versus control; Fig. 6a-b) associated with an unchanged total branch length per mitochondrion (Fig. 6a-b).

Interestingly, A-172 cells were not affected by GA treatment in their total number of mitochondrial particles (Fig. 6c-d), showing a reduction in total branch length per mitochondrion (0.56 ± 0.33 A-172 + GA, FC versus control; Fig. 6c-d). Mitochondrial parameters in CCF-STTG1 cells were also slightly affected by GA treatment, with a significant reduction of the number of mitochondrial individual particles (0.58 ± 0.20 CCF-STTG1 + GA, FC versus control; Fig. 6e-f) and no changes in the total branch length per mitochondrion (Fig. 6e-f). U-87 MG, characterised by stable mt-CX43 in response to pH alterations and reduced mt-CX43 upon GA treatment, showed no significant changes in mitochondrial morphological parameters in response to GA (Fig. 6g-h). To correlate the modulation of mt-CX43 with metabolic reprogramming associated with extracellular pH-mediated stress, we conducted a targeted metabolomics analysis (Fig. 7a). We first performed a PCA and extracted PC1 and PC2, which explained approximately 82.1% of the total variance (Figure S5). These data showed an apparent clustering of the tested cell lines exposed to pH = 8.0 and pH = 8.0 + GA, highlighting the impact of critical metabolites contributing to the clusters (Fig. 7b-i, S5). Our data revealed that T98-G cells, which are susceptible to pH alterations and in which CX43 plays a role in mitochondrial morphological changes, responded to GA-mediated mt-CX43 reduction by significantly increasing the levels of IMP (0.58 ± 0.07 GA vs. 0.29 ± 0.02 control, nmol/1 × 10^6 cells, Fig. 7b), and uracil (0.0089 ± 0.0022

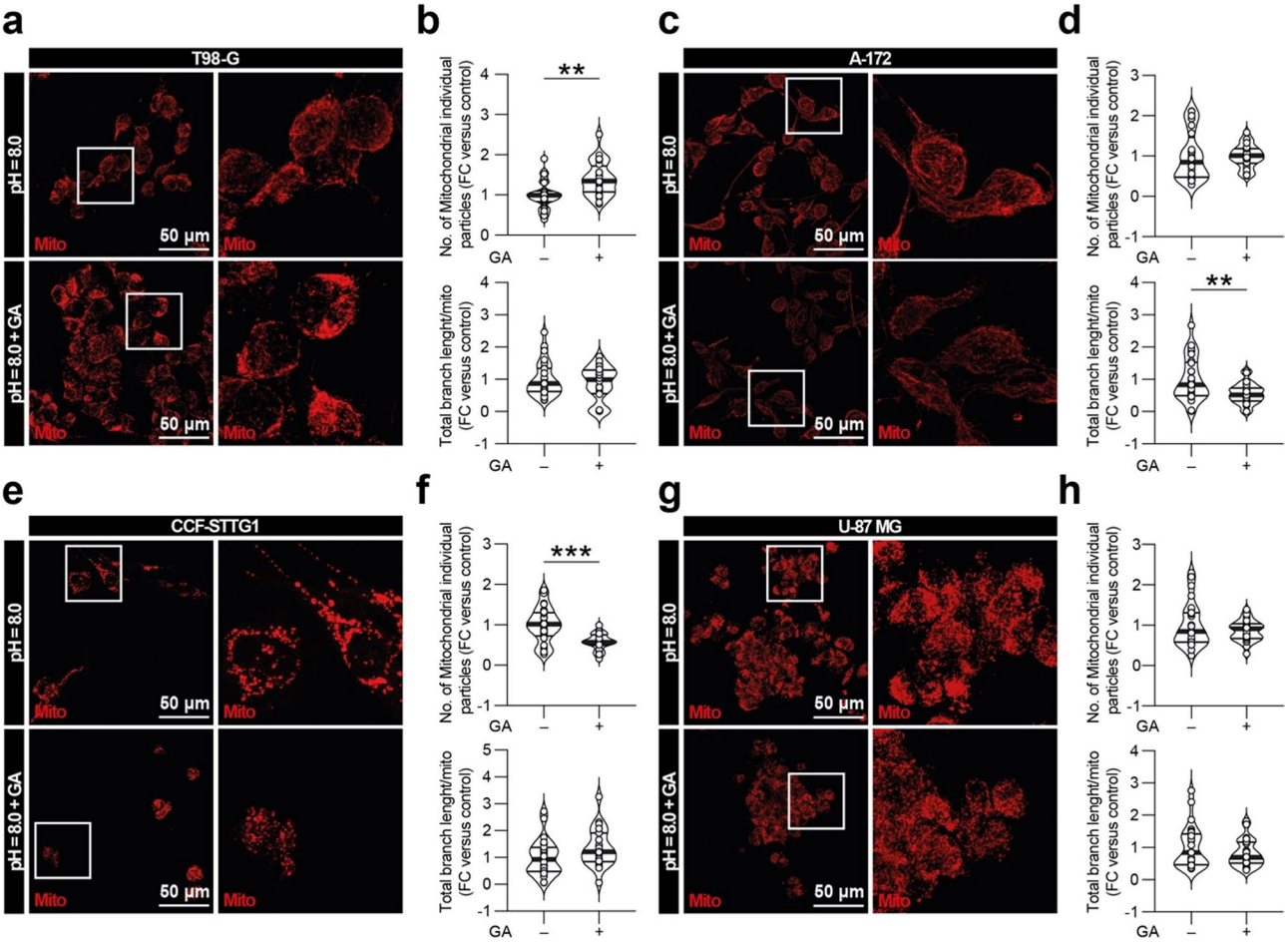

Fig. 6 Geldanamycin induces remodelling of mitochondrial morphological parameters. **a**-**b** Representative confocal images of Mito (red) in control and GA T98-G cells (**a**) and quantification of the number of individual mitochondrial particles and the total branch length per mito (**b**). **c**-**d** Representative confocal images of Mito (red) in control and GA A-172 cells (**c**) and quantification of the number of individual mitochondrial particles and the total branch length per mito (**d**). **e**-**f** Representative confocal images of Mito (red) in control and GA CCF-STTG1 cells (**e**) and quantification of the number of individual mitochondrial particles and the total branch length per mito (**f**). **g**-**h** Representative confocal images of Mito (red) in control and GA U-87 MG cells (**g**) and quantification of the number of individual mitochondrial particles and the total branch length per mito (**h**). Data in (**b**, **d**, **f**, and **h**) are expressed as FC versus control and shown as dot plot and violin plot, with the middle line representing the median and the thin lines the quartiles from $n \geq 3$ biological replicates. **p-value < 0.01; ***p-value < 0.001. Mito: mitochondrial marker; GA: geldanamycin; FC: fold change

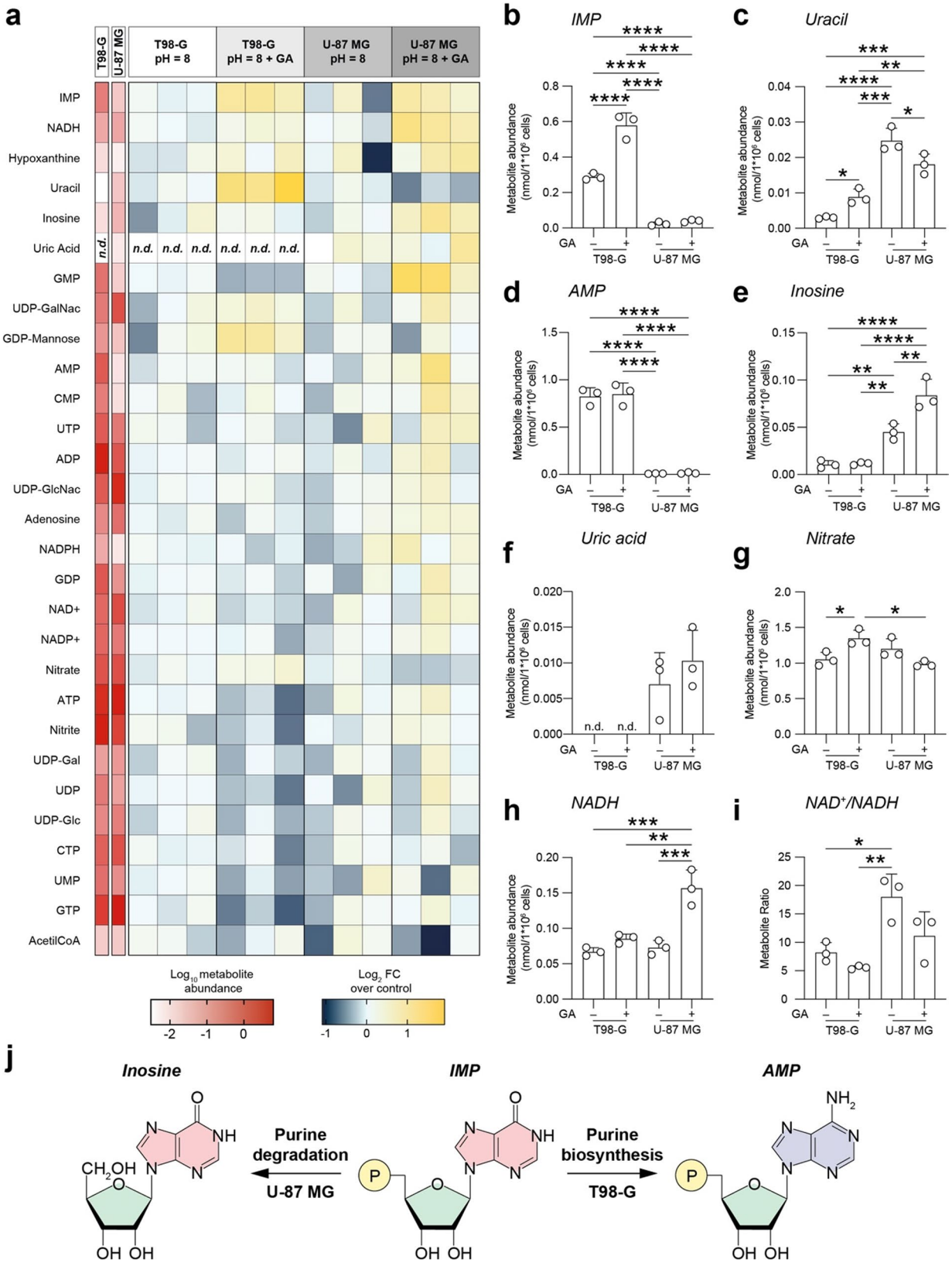

Fig. 7 (See legend on next page.)

(See figure on previous page.)

Fig. 7 Altered mitochondrial CX43 levels induce opposite metabolic shifts in T98-G and U-87 MG cells. **a** Heatmap of 29 metabolites showing their abundance and the relative changes in T98-G cells at pH = 8.0, T98-G cells at pH = 8.0 + GA, U-87 MG cells at pH = 8.0, and U-87 MG cells at pH = 8.0 + GA. Data are shown as $\log_{10}$ metabolite abundance and $\log_2$ FC versus control pH = 8.0 from $n = 3$ biological replicates. b-h) Abundance of IMP (**b**), uracil (**c**), AMP (**d**), inosine (**e**), uric acid (**f**), nitrate (**g**), NADH (**h**) in T98-G cells at pH = 8.0, T98-G cells at pH = 8.0 + GA, U-87 MG cells at pH = 8.0, and U-87 MG cells at pH = 8.0 + GA. Data are expressed as dot plots and mean ± SD of metabolite abundance in nmol per 1×10^6 cells from $n = 3$ biological replicates. **i** Ratio between metabolite abundances of NAD^+/NADH in T98-G cells at pH = 8.0, T98-G cells at pH = 8.0 + GA, U-87 MG cells at pH = 8.0, and U-87 MG cells at pH = 8.0 + GA. Data are presented as dot plots and mean ± SD of ratios from $n = 3$ biological replicates. *p-value < 0.05; **p-value < 0.01; ***p-value < 0.001; ****p-value < 0.0001. **j** Schematic representation of the metabolic pathways differentially affected by GA in T98-G and U-87 MG cells. GA: geldanamycin; n.d.: not detected; FC: fold change.

GA vs. 0.0030 ± 0.0003 control, nmol/1×10^6 cells, Fig. 7c), with stable high levels of AMP (0.85 ± 0.12 GA T98-G vs. 0.83 ± 0.09 control T98-G, nmol/1×10^6 cells, Fig. 7d) and reduced inosine (0.012 ± 0.001 GA T98-G vs. 0.011 ± 0.003 control T98-G, nmol/1×10^6 cells, Fig. 7e), compared to U-87 MG cells (AMP: 0.015 ± 0.007 GA U-87 MG vs. 0.009 ± 0.002 control U-87 MG, nmol/1×10^6 cells, Fig. 7d; inosine: 0.084 ± 0.017 GA U-87 MG vs. 0.045 ± 0.008 control U-87 MG, nmol/1×10^6 cells, Fig. 7e). Interestingly, GA treatment decreased the levels of uracil in U-87 MG cells (0.0181 ± 0.0029 GA vs. 0.0248 ± 0.0035 control, nmol/1×10^6 cells, Fig. 7c) with a significant increase of inosine (Fig. 7e).

Concomitantly, T98-G cells showed undetectable levels of uric acid (Fig. 7f) and significantly increased nitrosative stress (nitrate: 1.35 ± 0.12 GA vs. 1.06 ± 0.10 control, nmol/1×10^6 cells, Fig. 7g), while U-87 MG showed a slight decrease in nitrate levels under GA treatment (0.99 ± 0.04 GA vs. 1.20 ± 0.14 control, nmol/1×10^6 cells, Fig. 7g).

Quantitative analysis of metabolites in U-87 MG cells revealed a substantial increase in NADH (0.16 ± 0.03 GA vs. 0.07 ± 0.01 control, nmol/1×10^6 cells; Fig. 7h) coupled with a slight but non-significant reduction in the NAD^+/NADH ratio (11.16 ± 4.21 GA vs. 18.02 ± 3.98 control, ratio; Fig. 7i).

To strengthen our evidence, we analysed purine metabolite ratios via the adenylic ratio [(AMP + IMP)/(adenosine + inosine + hypoxanthine + uric acid)], IMP turnover [(IMP)/(inosine + hypoxanthine + uric acid)], and guanylic ratio [(GMP + IMP)/(guanosine + inosine + hypoxanthine + uric acid)] (Figure S5). We found significantly higher ratios in T98-G cells compared to U-87 MG cells (Figure S5). Moreover, our analysis revealed that GA-induced mt-CX43 reduction mediates a significant increase in the adenylic ratio (6.94 ± 1.20 GA vs. 5.20 ± 0.47 control; Figure S5) and IMP turnover (22.17 ± 4.39 GA vs. 14.01 ± 4.14 control; Figure S5) in T98-G cells. While we observed no significant changes in the guanylic ratio between control and GA-treated T98-G and U-87 MG cells (Figure S5).

Collectively, these findings indicate increased purine biosynthesis in T98-G cells and increased purine degradation in U-87 MG cells (Fig. 7j), with recovery after stress and metabolic reprogramming due to increased NADH levels in U-87 MG, suggesting a rearrangement of glycolysis and mitochondrial metabolism.

Discussion

CX43 is one of the most abundant GJ-forming proteins, playing an essential role in mediating intercellular communication [34, 35]. By assembling into HCs and GJs, this protein enables the direct transfer of ions and small molecules between the cytosol and extracellular space, and between adjacent cells, respectively, thereby contributing to cellular homeostasis [5, 36]. Alongside its well-established canonical roles, the non-canonical functions of CX43 have gained increasing attention, suggesting that this protein may contribute to physiological processes beyond the traditional GJ-forming proteins [37, 38]. These include regulation of cell proliferation, apoptosis and involvement in inflammatory responses [39–41]. Notably, CX43 has also been found inside mitochondria, where previous studies in cardiomyocytes and the heart have demonstrated a pivotal role in metabolism, oxidative stress response and mitochondrial activity [10, 11]. However, while the role of CX43 in GJ-mediated intercellular communication has been extensively studied over several decades, the presence and activity of CX43 in mitochondria are a very recent discovery and many aspects remain to be further addressed and investigated.

The first study demonstrating the presence of CX43 within mitochondria was conducted by Boengler et al. in cardiomyocytes, where CX43 was isolated from mitochondrial fractions [8]. The authors demonstrated that mt-CX43 can regulate mitochondrial potassium influx and contribute to cardioprotection during ischemic preconditioning [8]. Subsequent studies corroborated these findings and proposed a mechanism for CX43 import into mitochondria, involving HSP90 and the translocase of the outer membrane TOM complex [42, 43].

From a functional perspective, mt-CX43 has been identified as a significant contributor to diazoxide-induced cardioprotection. Its reduction has been shown to impact ADP-stimulated respiration and to decrease the respiratory control ratio, confirming the influence of mt-CX43 on mitochondrial bioenergetics [9]. In addition to respiration, mt-CX43 has been shown to influence mitochondrial volume and ROS production [44]. These findings further support the hypothesis that mt-CX43-based

HCs mainly remain closed under homeostatic conditions to prevent dissipation of the membrane potential, but transiently open under stress to enhance metabolic adaptation [9, 45]. Regarding its function in neural cells, although CX43 is the most abundantly expressed CX, and is involved in key physiological and pathological processes such as astrocyte-neuron communication, cell proliferation, and neuroinflammation, the role of mt-CX43 in the CNS remains largely unexplored. An important in vivo study by Hou et al. addressed this gap by demonstrating that mt-CX43 accumulates in the mitochondria of neurovascular unit cells following cerebral ischemia-reperfusion injury in rats [46]. These findings revealed that mt-Cx43 contributes to neuroprotection by maintaining the mitochondrial membrane potential, reducing ROS production, and limiting cell injury, in line with previously observed mechanisms in models of cardiovascular diseases [46].

Herein, we first investigated the shuttling of mt-CX43 into the mitochondria of four selected glioma cell lines, and we describe how environmental and cellular conditions dynamically regulate this process. Specifically, we showed that T98-G cells, which are characterised by low basal CX43 expression, display minimal mt-CX43 levels that further decrease under HD, while U-87 MG cells, which have high endogenous CX43 protein levels, upregulate mt-CX43 under HD conditions. These findings suggest that the basal CX43 expression and cell confluence are significant determinants of mitochondrial localisation of CX43, opening new avenues for studying the intracellular trafficking and function of this protein in CNS cell populations.

In addition to examining mitochondrial localisation, we also evaluated the distribution of CX43 in other subcellular compartments, namely the subplasmalemmal region and the nuclear compartment, to better frame its functional plasticity. As expected, CX43 was abundant in the subplasmalemmal region, particularly in A-172 and CCF-STTG1 cells seeded in HD, consistent with its role as HC- and GJ-forming protein [47, 48]. Interestingly, we also detected a marked nuclear localisation of CX43 in CCF-STTG1 cells, confirming reports that correlate nuclear CX43 with transcriptional modulatory functions [49, 50]. These observations provide further interesting insights into CX43 and strengthen the idea that its localisation at the subcellular level is tightly controlled and relevant for its function. From this perspective, the presence of CX43 in the mitochondria is an intriguing aspect, suggesting that glioma cells may utilise the CX43 pool to coordinate their response to stress at multiple cellular levels. CX43 is not restricted to a specific compartment but appears to function as a multi-organelle protein, potentially enabling glioma cells to orchestrate complex responses to environmental stressors. To further investigate mt-CX43-mediated modulation of the mitochondrial network, we evaluated morphological markers of fusion and fission as a function of cell density. Interestingly, we observed cell line–specific differences by detecting increased mitochondrial fusion in HD T98-G cells, whereas mitochondrial fission was observed in U-87 MG cells. This opposing behaviour suggests that cells preferentially activate mitochondrial remodelling strategies depending on baseline CX43 levels under similar environmental conditions. This divergence may reflect intrinsic differences in their bioenergetic profiles or stress adaptation mechanisms.

To explore potential metabolic regulators of mitochondrial CX43 translocation, we assessed the effects of lactate-induced modulation of mitochondrial dynamics [51–53]. However, following lactate exposure, we did not observe significant differences in mt-CX43 levels in the tested cell lines. These findings suggest that, although lactate can modulate mitochondrial morphology and function, it does not appear to have a significant effect on the mitochondrial localisation of CX43. Since our observations provided direct evidence for the presence of CX43 in the mitochondria, we decided to modulate its translocation from the cytoplasm to the mitochondria, by treating the cells with GA, a known inhibitor of the HSP90 chaperone system that impairs protein folding and prevents the correct binding of the protein to the mitochondria by the TOM translocation complex [27]. GA is a broad-spectrum inhibitor of HSP90, thus exerting pleiotropic and off-target effects on a wide range of proteins which could be directed from the cytoplasm to the mitochondria [54]. In this work, we tried to minimise potential off-target effects by using a concentration of 10 μM and an exposure time of 30 min, taking into account the short half-life of CX43, which undergoes rapid turnover [55].

Our results, demonstrating that GA significantly reduced the expression of mt-CX43, are in line with previous studies on cells isolated from rat hearts, which showed mitochondrial localisation of CX43. In particular, localisation of mt-CX43 in the inner mitochondrial membrane follows translocation via the TOM complex [27]. To date, the effects of GA treatment on glioma cell lines exposed to alterations in extracellular pH have not been investigated. Our work suggests that mt-CX43 is imported by a chaperone-mediated mechanism that is actively used by the cell to support the entry of CX43 into mitochondria. Interestingly, these effects were observed after a short treatment with GA (i.e., 30 min post-treatment). This rapid reduction in mt-CX43 levels suggests a CX43 turnover between the cell cytoplasm and mitochondria, which may also be linked to the short half-life of CX43 [55, 56]. Moreover, this study supports a direct

involvement of mt-CX43 and metabolic alterations associated with extracellular pH fluctuations.

To correlate the modulation of mt-CX43 with metabolic reprogramming associated with extracellular pH-mediated stress, we analysed the metabolic differences between T98-G and U-87 MG cells exposed to pH = 8.0 and pH = 8.0 + GA. The tumour microenvironment is typically characterised by an acidic extracellular pH, which is a central hallmark of glioma biology and is well known to regulate proliferation and resistance to therapies [57]. For this reason, we initially tested both acidic (pH 6.0) and alkaline (pH 8.0) conditions to reproduce a wide range of extracellular fluctuations. Our results indicated that acidification reduced the mitochondrial translocation of CX43 in T98-G but not in U-87 MG cells, whereas alkalinisation induced an accumulation of mt-CX43. This observation prompted us to investigate further the alkaline conditions to uncover the biological mechanisms related to mt-CX43 shuttling within mitochondria. However, it is important to emphasise that, although extracellular acidosis is the prevailing state in gliomas, localised fluctuations towards more alkaline values may occur, especially in intracellular pH [58]. Such microenvironmental heterogeneity may contribute to glioma metabolic plasticity and provide a rationale for exploring both acidic and alkaline shifts in relation to mt-CX43. Direct assessment of intracellular pH would therefore be an important next step in understanding how intracellular homeostasis intersects with mitochondrial CX43 trafficking and function.

In T98-G cells, which showed low basal CX43 expression and reduced mt-CX43 levels under HD stress, we observed a marked accumulation of purine and pyrimidine intermediates, including IMP and uracil, after GA treatment. Elevated levels of IMP suggest upregulation of the purine biosynthetic pathway. This hypothesis is also supported by the unchanged level of inosine in T98-G cells, implying that IMP serves as a precursor for purine biosynthesis, rather than a product of its degradation. We have recently found that purine metabolism is associated with tumour proliferation and resistance to chemotherapy, with the combined approach of guanosine and inosine with temozolomide improving chemotherapy efficacy in GBM cell lines [59]. Accumulation of uracil may indicate increased replication stress and impaired DNA repair, possibly due to misincorporation of uracil into DNA or disruption of polymerase function [60]. Increased nitrate levels may indicate an enhanced nitric oxide metabolism and oxidative stress, which further support the hypothesis of activation of redox stress adaptation mechanisms in the absence of mt-CX43.

In U-87 MG cells exposed to GA, we observed a reduction in uracil levels in contrast to the T98-G results, indicating a different metabolic response. Moreover, we observed a significant increase in NADH levels with a stable NAD^+/NADH ratio. Higher NADH levels indicate increased glycolysis, potentially reflecting a metabolic reprogramming under metabolic stress [61, 62]. T98-G cells, which express low levels of CX43 at baseline, seem to depend on mt-CX43 to enhance anabolic purine metabolism. U-87 MG cells, on the other hand, contain high levels of CX43 at baseline and shift to increased NADH production, in line with their more glycolytic, stress-tolerant nature and increased purine degradation. These differences may rely on the intrinsic metabolic reprogramming and suggest that mt-CX43 contributes to tumour heterogeneity. Glioma cells undergo metabolic reshaping to produce specific metabolites that promote the invasion and proliferation of healthy tissue. Therefore, the observed differences following mt-CX43 variations should be considered, as these may represent potential targets for novel therapeutic strategies.

From a translational perspective, our findings indicate that mt-CX43 may play a role in the stress adaptation of gliomas and may represent a potential vulnerability in tumour biology. Targeting mt-CX43 could disrupt glioma metabolic adaptability, a major driver of therapy resistance and tumour recurrence.

Conclusions

Our results support a correlation between mt-CX43 and metabolic adaptation in response to stress in glioma cell lines. Indeed, we provide evidence for the regulation of mt-CX43 expression by cell density, extracellular pH fluctuations, and protein turnover between the cytoplasm and mitochondria via chaperone-mediated import. Significantly, the reduction of mt-CX43 by GA was associated with changes in mitochondrial morphological parameters and cell line-specific metabolic changes. In T98-G cells, the reduction in mt-CX43 was associated with a stress-adaptive phenotype. Conversely, U-87 MG cells showed more pronounced metabolic reprogramming, which may be associated with increased tumour aggressiveness. These findings highlight the importance of CX43 compartmentalisation, especially within mitochondria, which is emerging as a critical determinant of glioma stress adaptation. This work supports the hypothesis that the modulation of mt-CX43 may represent a novel target for metabolic reprogramming to develop more effective and personalised treatments for glioma. Our findings expand the understanding of CX43 beyond its canonical role in GJs by highlighting its capacity to function as a multi-compartmental signalling protein that integrates mitochondrial activity, metabolic plasticity, and stress adaptation.

Abbreviations

CCLE	Cancer Cell Line Encyclopedia
CNS	Central nervous system
Cos^2	Squared cosine
CX	Connexin
CX43	Connexin 43
DMEM	Dulbecco's Modified Eagle Medium
DMSO	Dimethyl sulfoxide
FBS	Foetal bovine serum
FC	Fold change
GA	Geldanamycin
GBM	Glioblastoma
GJ	Gap junction
HC	Hemichannel
HD	High density
HPLC	High-performance liquid chromatography
HSP90	Heat shock protein 90
LD	Low density
MD	Medium plating density
MEM	Minimum essential medium
Mito	Mitochondrial marker
mt-CX43	Mitochondrial Connexin 43
NGS	Normal goat serum
PC	Principal component
PCA	Principal component analysis
PFA	Paraformaldehyde
PHD	Phalloidin
PKA	Protein kinase A
RPKM	Reads per kilobase of transcript per million mapped reads
ROI	Region of interest
ROS	Reactive oxygen species
TOM	Translocase of the outer membrane

Supplementary Information

The online version contains supplementary material available at https://doi.org/10.1186/s12964-025-02523-2.

Supplementary Material 1.

Supplementary Material 2.

Acknowledgements

The authors would like to thank the confocal microscopy facility at the Bio-Nanotech Research and Innovation Tower (BRIT) of the University of Catania and all the members of the Laboratory of Cellular and Molecular Physiology, for their technical contributions. A.G. and S.Den. were supported by the Ph.D. program in Biotechnology (Department of Biomedical and Biotechnological Sciences, University of Catania, Italy).

Authors' contributions

Conceptualisation: R.P., N.V.; methodology: A.G., S.Denaro, S.D'Aprile, M.P., J.J., R.Z., D.T., A.M.A., R.P., N.V.; investigation: A.G., S.Denaro, S.D'Aprile, A.M.A., N.V.; data curation: A.G., A.M.A., A.Z., R.P., N.V.; formal analysis: all authors; writing-original draft: A.G., R.P., N.V.; writing-review and editing: all authors. project administration: R.P., N.V.; all the authors read and approved the final manuscript.

Funding

This study was partially funded by the grant Piano di Incentivi per la Ricerca di Ateneo 2020–2022 - PIA.CE.RI. 2020–2022-Linea di intervento 3-Starting Grant, CHRONOS and by the grant Piano di Incentivi per la Ricerca di Ateneo 2024–2026 - PIA.CE.RI. 2024–2026-Linea di intervento 1, ACHIEVE from the University of Catania to NV. This study was also partially funded by the grant National Biodiversity Future Center (NBFC) by the European Union NextGenerationEU, PNRR, project n. CN00000033; CUP: E63C22004340006; META-CONNECT–Spoke 6 and by the National Plan for NRRP Complementary Investments (PNC, established with the decree-law 6 May 2021, n. 59, converted by law n. 101 of 2021) in the call for the funding of research initiatives for technologies and innovative trajectories in the health and care sectors (Directorial Decree n. 931 of 06-06-2022)—project n. PNC0000003—AdvaNced Technologies for Human-centrEd Medicine (project acronym: ANTHEM). This work reflects only the authors' views and opinions, neither the Ministry for University and Research nor the European Commission can be considered responsible for them.
This work was supported by the Slovenian Research Agency (grant numbers P3 310, J7-3153, I0-0034, I0-0048 (CIPKeBiP), I0-0022 (MRIC UL), and J4-60077), EU Interreg Italia-Slovenia Immunocluster-2, EU Interreg Italia-Slovenia Coherence, and the A4L_ACTIONS and A4L_BRIDGE projects funded by the European Union's Horizon 2020 (grant agreement no. 101136453).

Data availability

All data generated or analysed during this study are included in this published article and its supplementary information files.

Declarations

Ethics approval and consent to participate

Not applicable.

Consent for publication

Not applicable.

Competing interests

The authors declare no competing interests.

Author details

[1]Section of Physiology, Department of Biomedical and Biotechnological Sciences, University of Catania, Catania 95123, Italy
[2]Department of Medicine and Surgery, University of Enna "Kore", Enna 94100, Italy
[3]Laboratory of Neuroendocrinology-Molecular Cell Physiology, Institute of Pathophysiology, Faculty of Medicine, University of Ljubljana, Ljubljana 1000, Slovenia
[4]Celica Biomedical, Ljubljana, Slovenia
[5]Section of Biochemistry, Department of Biomedical and Biotechnological Sciences, University of Catania, Catania 95123, Italy

Received: 18 August 2025 / Accepted: 31 October 2025
Published online: 27 November 2025

References

1. Sohl G, Willecke K. Gap junctions and the connexin protein family. Cardiovasc Res. 2004;62(2):228–32.
2. van Zeijl L, Ponsioen B, Giepmans BN, Ariaens A, Postma FR, Varnai P, et al. Regulation of connexin43 gap junctional communication by phosphatidylinositol 4,5-bisphosphate. J Cell Biol. 2007;177(5):881–91.
3. Goodenough DA, Paul DL. Gap junctions. Cold Spring Harb Perspect Biol. 2009;1(1):a002576.
4. Giaume C, Naus CC, Saez JC, Leybaert L. Glial connexins and pannexins in the healthy and diseased brain. Physiol Rev. 2021;101(1):93–145.
5. Vicario N, Parenti R. Connexins signatures of the neurovascular unit and their physio-pathological functions. Int J Mol Sci. 2022. https://doi.org/10.3390/ijms23179510.
6. Denaro S, D'Aprile S, Vicario N, Parenti R. Mechanistic insights into connexin-mediated neuroglia crosstalk in neurodegenerative diseases. Front Cell Neurosci. 2025;19:1532960.
7. Zhang J, Riquelme MA, Hua R, Acosta FM, Gu S, Jiang JX. Connexin 43 hemichannels regulate mitochondrial ATP generation, mobilization, and mitochondrial homeostasis against oxidative stress. Elife. 2022. https://doi.org/10.7554/eLife.82206.
8. Boengler K, Dodoni G, Rodriguez-Sinovas A, Cabestrero A, Ruiz-Meana M, Gres P, et al. Connexin 43 in cardiomyocyte mitochondria and its increase by ischemic preconditioning. Cardiovasc Res. 2005;67(2):234–44.
9. Ruiz-Meana M, Rodriguez-Sinovas A, Cabestrero A, Boengler K, Heusch G, Garcia-Dorado D. Mitochondrial connexin43 as a new player in the pathophysiology of myocardial ischaemia-reperfusion injury. Cardiovasc Res. 2008;77(2):325–33.
10. Boengler K, Schulz R. Connexin 43 and mitochondria in cardiovascular health and disease. Adv Exp Med Biol. 2017;982:227–46.

11. Boengler K, Leybaert L, Ruiz-Meana M, Schulz R. Connexin 43 in mitochondria: what do we really know about its function? Front Physiol. 2022;13:928934.
12. Flavahan WA, Wu Q, Hitomi M, Rahim N, Kim Y, Sloan AE, et al. Brain tumor initiating cells adapt to restricted nutrition through preferential glucose uptake. Nat Neurosci. 2013;16(10):1373–82.
13. Jawhari S, Ratinaud MH, Verdier M. Glioblastoma, hypoxia and autophagy: a survival-prone 'menage-a-trois.' Cell Death Dis. 2016;7(10):e2434.
14. Seyfried TN, Arismendi-Morillo G, Zuccoli G, Lee DC, Duraj T, Elsakka AM, et al. Metabolic management of microenvironment acidity in glioblastoma. Front Oncol. 2022;12:968351.
15. D'Aprile S, Denaro S, Gervasi A, Vicario N, Parenti R. Targeting metabolic reprogramming in glioblastoma as a new strategy to overcome therapy resistance. Front Cell Dev Biol. 2025;13:1535073.
16. Sin WC, Crespin S, Mesnil M. Opposing roles of connexin43 in glioma progression. Biochim Biophys Acta. 2012;1818(8):2058–67.
17. Smyth JW, Guo S, Chaunsali L, O'Rourke L, Dahlka J, Deaver S, et al. Cytoplasmic connexin43-microtubule interactions promote glioblastoma stem-like cell maintenance and tumorigenicity. Cell Death Dis. 2025;16(1):388.
18. Hitomi M, Deleyrolle LP, Mulkearns-Hubert EE, Jarrar A, Li M, Sinyuk M, et al. Differential connexin function enhances self-renewal in glioblastoma. Cell Rep. 2015;11(7):1031–42.
19. Ye XY, Jiang QH, Hong T, Zhang ZY, Yang RJ, Huang JQ, et al. Altered expression of connexin43 and phosphorylation connexin43 in glioma tumors. Int J Clin Exp Pathol. 2015;8(5):4296–306.
20. Zhang M, Wang ZZ, Chen NH. Connexin 43 phosphorylation: implications in multiple diseases. Molecules. 2023. https://doi.org/10.3390/molecules28134914.
21. Johnson KE, Mitra S, Katoch P, Kelsey LS, Johnson KR, Mehta PP. Phosphorylation on Ser-279 and Ser-282 of connexin43 regulates endocytosis and gap junction assembly in pancreatic cancer cells. Mol Biol Cell. 2013;24(6):715–33.
22. Duffy HS, Sorgen PL, Girvin ME, O'Donnell P, Coombs W, Taffet SM, et al. pH-dependent intramolecular binding and structure involving Cx43 cytoplasmic domains. J Biol Chem. 2002;277(39):36706–14.
23. Sorgen PL, Duffy HS, Spray DC, Delmar M. pH-dependent dimerization of the carboxyl terminal domain of Cx43. Biophys J. 2004;87(1):574–81.
24. Hirst-Jensen BJ, Sahoo P, Kieken F, Delmar M, Sorgen PL. Characterization of the pH-dependent interaction between the gap junction protein connexin43 carboxyl terminus and cytoplasmic loop domains. J Biol Chem. 2007;282(8):5801–13.
25. Tafech A, Jacquet P, Beaujean C, Fertin A, Usson Y, Stephanou A. Characterization of the intracellular acidity regulation of brain tumor cells and consequences for therapeutic optimization of Temozolomide. Biology. 2023. https://doi.org/10.3390/biology12091221.
26. Yamaguchi DT, Ma D. Mechanism of pH regulation of connexin 43 expression in MC3T3-E1 cells. Biochem Biophys Res Commun. 2003;304(4):736–9.
27. Rodriguez-Sinovas A, Boengler K, Cabestrero A, Gres P, Morente M, Ruiz-Meana M, et al. Translocation of connexin 43 to the inner mitochondrial membrane of cardiomyocytes through the heat shock protein 90-dependent TOM pathway and its importance for cardioprotection. Circ Res. 2006;99(1):93–101.
28. Yang F, Chen WL, Zheng MZ, Yu GW, Xu HJ, Shen YL, et al. Heat shock protein 90 mediates anti-apoptotic effect of diazoxide by preventing the cleavage of bid in hypothermic preservation rat hearts. J Heart Lung Transplant. 2011;30(8):928–34.
29. D'Aprile S, Denaro S, Pavone AM, Giallongo S, Giallongo C, Distefano A, et al. Anaplastic thyroid cancer cells reduce CD71 levels to increase iron overload tolerance. J Transl Med. 2023;21(1):780.
30. Denaro S, D'Aprile S, Torrisi F, Zappala A, Marrazzo A, Al-Khrasani M, et al. Sigma-1 receptor targeting inhibits connexin 43 based intercellular communication in chronic neuropathic pain. Inflamm Res. 2024;73(10):1711–26.
31. Schindelin J, Arganda-Carreras I, Frise E, Kaynig V, Longair M, Pietzsch T, et al. Fiji: an open-source platform for biological-image analysis. Nat Methods. 2012;9(7):676–82.
32. Chaudhry A, Shi R, Luciani DS. A pipeline for multidimensional confocal analysis of mitochondrial morphology, function, and dynamics in pancreatic beta-cells. Am J Physiol Endocrinol Metab. 2020;318(2):E87-101.
33. Morley GE, Taffet SM, Delmar M. Intramolecular interactions mediate pH regulation of connexin43 channels. Biophys J. 1996;70(3):1294–302.
34. Kar R, Batra N, Riquelme MA, Jiang JX. Biological role of connexin intercellular channels and hemichannels. Arch Biochem Biophys. 2012;524(1):2–15.
35. Ribeiro-Rodrigues TM, Martins-Marques T, Morel S, Kwak BR, Girao H. Role of connexin 43 in different forms of intercellular communication - gap junctions, extracellular vesicles and tunnelling nanotubes. J Cell Sci. 2017;130(21):3619–30.
36. De Maio A, Vega VL, Contreras JE. Gap junctions, homeostasis, and injury. J Cell Physiol. 2002;191(3):269–82.
37. Van Campenhout R, Cooreman A, Leroy K, Rusiecka OM, Van Brantegem P, Annaert P, et al. Non-canonical roles of connexins. Prog Biophys Mol Biol. 2020;153:35–41.
38. Paunikar S, Tamagnone L. Connexin-43 in cancer: above and beyond gap junctions! Cancers (Basel). 2024. https://doi.org/10.3390/cancers16244191.
39. Chevallier D, Carette D, Segretain D, Gilleron J, Pointis G. Connexin 43 a checkpoint component of cell proliferation implicated in a wide range of human testis diseases. Cell Mol Life Sci. 2013;70(7):1207–20.
40. Xue J, Yan X, Yang Y, Chen M, Wu L, Gou Z, et al. Connexin 43 dephosphorylation contributes to arrhythmias and cardiomyocyte apoptosis in ischemia/reperfusion hearts. Basic Res Cardiol. 2019;114(5):40.
41. Li T, Niu J, Yu G, Ezan P, Yi C, Wang X, et al. Connexin 43 deletion in astrocytes promotes CNS remyelination by modulating local inflammation. Glia. 2020;68(6):1201–12.
42. Tu RH, Li QJ, Huang Z, He Y, Meng JJ, Zheng HL, et al. Novel functional role of heat shock protein 90 in mitochondrial connexin 43-mediated hypoxic postconditioning. Cell Physiol Biochem. 2017;44(3):982–97.
43. An L, Gao H, Zhong Y, Liu Y, Cao Y, Yi J, et al. Molecular chaperones HSP40, HSP70, STIP1, and HSP90 are involved in stabilization of Cx43. Cytotechnology. 2023;75(3):207–17.
44. Heinzel FR, Luo Y, Li X, Boengler K, Buechert A, Garcia-Dorado D, et al. Impairment of diazoxide-induced formation of reactive oxygen species and loss of cardioprotection in connexin 43 deficient mice. Circ Res. 2005;97(6):583–6.
45. Halestrap AP, Clarke SJ, Javadov SA. Mitochondrial permeability transition pore opening during myocardial reperfusion–a target for cardioprotection. Cardiovasc Res. 2004;61(3):372–85.
46. Hou S, Shen PP, Zhao MM, Liu XP, Xie HY, Deng F, et al. Mechanism of mitochondrial Connexin43's protection of the neurovascular unit under acute cerebral ischemia-reperfusion injury. Int J Mol Sci. 2016. https://doi.org/10.3390/ijms17050679.
47. Epifantseva I, Shaw RM. Intracellular trafficking pathways of Cx43 gap junction channels. Biochimica et Biophysica Acta (BBA). 2018;1860(1):40–7.
48. McCutcheon S, Spray DC. Glioblastoma-Astrocyte connexin 43 gap junctions promote tumor invasion. Mol Cancer Res. 2022;20(2):319–31.
49. Martins-Marques T, Witschas K, Ribeiro I, Zuzarte M, Catarino S, Ribeiro-Rodrigues T, et al. Cx43 can form functional channels at the nuclear envelope and modulate gene expression in cardiac cells. Open Biol. 2023;13(11):230258.
50. Dang X, Doble BW, Kardami E. The carboxy-tail of connexin-43 localizes to the nucleus and inhibits cell growth. Mol Cell Biochem. 2003;242(1–2):35–8.
51. Hu J, Cai M, Shang Q, Li Z, Feng Y, Liu B, et al. Elevated lactate by high-intensity interval training regulates the hippocampal BDNF expression and the mitochondrial quality control system. Front Physiol. 2021;12:629914.
52. Longhitano L, Giallongo S, Orlando L, Broggi G, Longo A, Russo A, et al. Lactate rewrites the metabolic reprogramming of uveal melanoma cells and induces quiescence phenotype. Int J Mol Sci. 2022. https://doi.org/10.3390/ijms24010024.
53. Longhitano L, Vicario N, Forte S, Giallongo C, Broggi G, Caltabiano R, et al. Lactate modulates microglia polarization via IGFBP6 expression and remodels tumor microenvironment in glioblastoma. Cancer Immunol Immunother. 2023;72(1):1–20.
54. Neckers L, Blagg B, Haystead T, Trepel JB, Whitesell L, Picard D. Methods to validate Hsp90 inhibitor specificity, to identify off-target effects, and to rethink approaches for further clinical development. Cell Stress Chaperones. 2018;23(4):467–82.
55. Laird DW, Puranam KL, Revel JP. Turnover and phosphorylation dynamics of connexin43 gap junction protein in cultured cardiac myocytes. Biochem J. 1991;273(Pt 1):67–72.
56. Solan JL, Lampe PD. Connexin43 phosphorylation: structural changes and biological effects. Biochem J. 2009;419(2):261–72.

57. Ferrauto G, Di Gregorio E, Auboiroux V, Petit M, Berger F, Aime S, et al. CEST-MRI for glioma pH quantification in mouse model: validation by immunohistochemistry. NMR Biomed. 2018;31(11):e4005.
58. Paech D, Weckesser N, Franke VL, Breitling J, Gorke S, Deike-Hofmann K, et al. Whole-brain intracellular pH mapping of gliomas using high-resolution (31)P MR spectroscopic imaging at 7.0 T. Radiology: Imaging Cancer. 2024;6(1):e220127.
59. D'Aprile S, Denaro S, Torrisi F, Longhitano L, Giallongo S, Giallongo C, et al. Purine metabolism rewiring improves glioblastoma susceptibility to Temozolomide treatment. Cell Death Dis. 2025;16(1):336.
60. Mortusewicz O, Haslam J, Gad H, Helleday T. Uracil-induced replication stress drives mutations, genome instability, anti-cancer treatment efficacy, and resistance. Mol Cell. 2025;85(10):1897–906.
61. Schroeder A, Pointer K, Clark P, Datta R, Kuo J, Eliceiri K. Metabolic mapping of glioblastoma stem cells reveals NADH fluxes associated with glioblastoma phenotype and survival. J Biomed Opt. 2020;25(3):1–13.
62. Wang Y, Stancliffe E, Fowle-Grider R, Wang R, Wang C, Schwaiger-Haber M, et al. Saturation of the mitochondrial NADH shuttles drives aerobic Glycolysis in proliferating cells. Mol Cell. 2022;82(17):3270–e839.

Publisher's Note

Springer Nature remains neutral with regard to jurisdictional claims in published maps and institutional affiliations.